IOP PUBLISHING JOURNAL OF PHYSICS D: APPLIED PHYSICS

J. Phys. D: Appl. Phys. **43** (2010) 185206 (12pp) doi:10.1088/0022-3727/43/18/185206

Intracellular electric fields produced by dielectric barrier discharge treatment of skin

Natalia Yu Babaeva and Mark J Kushner[1]

University of Michigan, Department of Electrical Engineering and Computer Science, 1301 Beal Ave., Ann Arbor, MI 48109, USA

E-mail: nbabaeva@umich.edu and mjkush@umich.edu

Received 1 February 2010, in final form 22 March 2010
Published 21 April 2010
Online at stacks.iop.org/JPhysD/43/185206

Abstract

The application of atmospheric pressure plasmas to human tissue has been shown to have therapeutic effects for wound healing and in treatment of skin diseases. These effects are attributed to both production of beneficial radicals which intersect with biological reaction chains and to the surface and intracellular generation of electric fields. In this paper, we report on computational studies of the intersection of plasma streamers in atmospheric pressure dielectric barrier discharges (DBDs) sustained in air with human skin tissue, with emphasis on the intracellular generation of electric fields. Intracellular structures and their electrical properties were incorporated into the computational mesh in order to self-consistently couple gas phase plasma transport with the charging of the surface of the skin and the intracellular production of electrical currents. The short duration of a single plasma filament in DBDs and its intersection with skin enables the intracellular penetration of electric fields. The magnitude of these electric fields can reach 100 kV cm^{-1} which may exceed the threshold for electroporation.

(Some figures in this article are in colour only in the electronic version)

1. Introduction

Non-equilibrium, atmospheric pressure plasma treatment of living tissue is being used in a variety of processes collectively called plasma medicine [1, 2]. These processes typically involve direct contact of a non-equilibrium plasma with biological cells resulting in, at one extreme, sterilization and, at the other extreme, therapeutic effects. These applications include disinfection [3], sterilization of food or living tissue without damage [4, 5], modulation of cell attachment [6–9], blood coagulation [10, 11], induction of apoptosis in malignant tissues [12] and wound healing [13]. The application of non-thermal air plasmas has also been shown to be effective in killing cancer cells [14, 15].

Two approaches are being followed in the use of non-thermal atmospheric pressure plasmas in medicine. In the first, the plasma is produced remotely, and its afterglow is delivered in a plume to the biological tissue. In this method, the sterilizing or therapeutic effects are likely produced by relatively long-lived neutral species as most of the charged particles do not survive outside the plasma generation region [16, 17]. In the second approach, plasmas are generated in direct contact with living tissue. When dielectric barrier discharges (DBDs) are used for this purpose, the plasma device typically contains the powered electrode while the tissue is the counter electrode. The fact that the DBD limits the current helps prevent the thermal damage of the tissue [9]. DBDs have been investigated in treating human skin and tissue in many contexts [10–13, 18–21]. Several technological challenges remain, including reproducibility due to the non-uniform filamentary structure of the plasma and sensitivity of the DBDs to the gap between the plasma applicator and the tissue. Larger filaments may produce localized heating and are typically concentrated in areas where the gap is smallest. However, the plasma can be tuned to achieve the desired medical effect, such as killing foreign organisms while not being harmful to the tissue [1, 13].

[1] Author to whom any correspondence should be addressed.

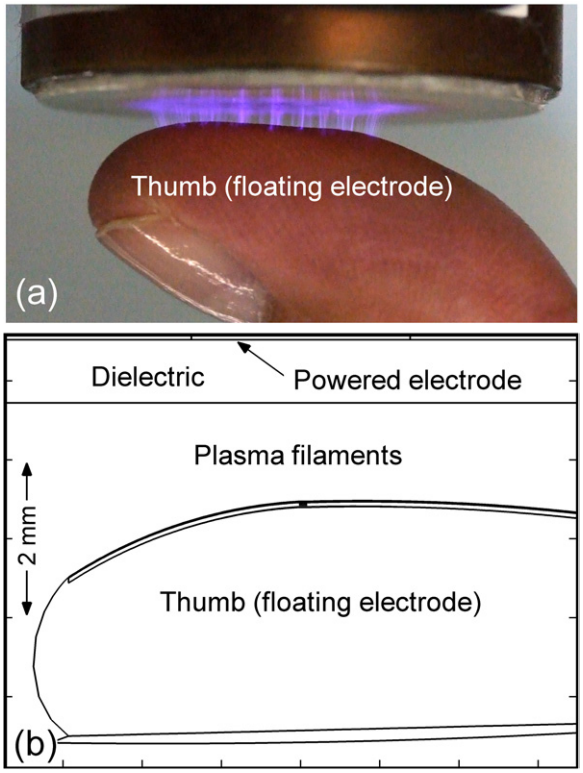

Figure 1. DBD treatment of human skin. (*a*) Plasma applied to a thumb acting as a floating electrode in a DBD in air (from [10]). (*b*) Schematic of the model geometry and computational domain. The upper powered electrode is covered with dielectric ($\varepsilon/\varepsilon_0 = 4$) and the bottom floating electrode is the thumb.

The therapeutic and sterilizing effects of plasmas, and those produced by DBDs in particular, may be attributed to several processes—production of fluxes of radicals and charged species onto cell surfaces, production of energetic fluxes of ions and photons impinging onto wounds and tissue surfaces, and generation of surface and intracellular electric fields. For example, NO which is produced in DBDs sustained in air, is known to promote and regulate wound healing [22, 23]. Similarly produced ozone inhibits the growth of cancerous cells [24] and ions improve blood coagulation. Electric fields of sufficient magnitude can initiate electroporation.

In this paper we focus on the latter effects—the production of large electric fields in the head of DBD filaments, the interaction of those fields with human skin cells, cell membranes and cell nuclei, and the intracellular production of electric fields through that interaction. Our modelling study addresses the experimental conditions of Fridman *et al* [10]—a non-thermal, room temperature DBD operating in open air with the plasma being in contact with human skin. (See figure 1(*a*).) In this configuration, the plasma applicator contains the powered electrode and the dielectric barrier. The counter electrode is the tissue being treated which has a high capacity for charge storage and to some degree acts as a floating electrode. The plasma is created in the gap between the powered, insulated electrode and the tissue. While the current in the gaseous discharge gap is mainly due to the motion of charge carriers, it continues mostly in the form of displacement current through the tissue.

Our investigation was conducted using a two-dimensional plasma hydrodynamics model. The cellular structure in the first 50–100 μm of human skin was incorporated into the computational mesh with permittivities and conductivities selected to represent the electrical properties of the intra- and inter-cell structures. As such, we model the propagation of the streamer across the gap, its intersection with skin, the charging of the surface of the skin and the generation of currents (conduction and displacement) and electric fields in the cells. We found that the short duration of the plasma filaments in DBDs enables significant penetration and production of electric fields within the conductive intracellular structures to levels exceeding 100 kV cm^{-1}. We relate these fields to prior studies of electroporation.

Brief overviews of conventional electroporation and supra-electroporation, and models addressing electroporation, are provided in section 2. The description of the model and our representation of human skin cells are given in section 3. The results of our modelling of a filamentary DBD are discussed in section 4. Results for cell charging and intracellular electric fields are given in section 5 followed by our concluding remarks in section 6.

2. Electroporation overview

The manner in which electric fields affect cells is determined by the interplay between their conductive cytoplasm and their surrounding dielectric-like cell membranes [25, 26]. When electric fields are applied to cells, the resulting current produces the accumulation of electric charges at the less conductive cell membranes which consequently leads to a voltage drop across the membrane. Conventional electroporation uses electric field pulses of tens of microseconds to milliseconds, durations that are longer than the cell membrane charging time. This produces a voltage of approximately 0.1–1 V across the membranes, which may cause structural changes and the formation of pores in the membrane. This is a useful tool in drug therapies because the pores typically reseal without directly detrimentally affecting the cell. Electroporation can be used to introduce water-soluble molecules into cells through these pores in the lipid bilayer of the cell membrane. The electric field plays the dual role of promoting pore formation and acting as a force to drive ions through the pores [27, 28].

The electric fields required for electroporation depend on the duration of the applied pulse. Schoenbach *et al* [29–31] studied structural and functional changes in human cells and solid tumors following exposure to high intensity (26–300 kV cm^{-1}) nanosecond pulsed electric fields in a process termed supra-electroporation. These pulses have been reported to initiate apoptosis in tumor cells and inhibit tumor growth. They found that in supra-electroporation, if the rise-time of the pulse is short compared with the dielectric relaxation time of the cell, electric fields propagate through cells, extensively penetrating organelles and involving all cell membranes. In conventional electroporation using pulses with longer rise-times, electric fields tend to propagate around conductive portions of cells and primarily affect the cell membranes.

Models of the interaction of cells with electric fields have used many approaches, starting with analytical models of electroporation [32, 33]. From an electrical viewpoint, a cell can be represented as a conducting medium surrounded by a lossy, dielectric envelope containing substructures having similar properties. In transport lattice models, equivalent circuits are used to describe the charging of the plasma membrane over the dielectric relaxation time, τ, of the membrane and that of the cytoplasm. Different circuit models are used for long pulses (pulse duration $> \tau$ of the plasma membrane) and short pulses (pulse duration $< \tau$ of cytoplasm generally < 1 ns for mammalian cells) [34, 35].

Molecular dynamics (MD) modelling of electroporation resolves cellular structure on an atomic basis. MD is computationally intensive and hence is typically restricted to more specialized studies of substructures of the cell over short periods [36–39]. For example, Joshi used 128 chains of lipid molecules and 3655 water molecules to model a patch of membrane of dimensions 4.5 nm, requiring time steps on the order of 1 fs [36, 37].

Bioelectric investigations have typically focused on the effects of electric fields on single, isolated cells [40]. These approaches are important to understand the details of intracellular processes. Models have also begun to investigate bioelectric effects at a higher level of discretization, including tissues, cell clusters and irregularly shaped cells [35, 40–43]. Issues still to be addressed include the cellular response to electric fields with regard to variability in cell density and shape, shape and randomness of the cellular clusters and the effects of heterogeneous tissue types.

3. Description of the model

In this study, a two-dimensional plasma hydrodynamics model was applied to the investigation of the propagation of plasma streamers in a DBD, their intersection with human skin and the generation of intracellular electric fields in the context of electroporation. The gas phase processes are represented using conventional plasma hydrodynamics equations including a full accounting of air plasma chemistry. The tissue is modelled as cell differentiated solids with appropriate permittivities and conductivities to represent, for example, cytoplasm and cell membranes. The plasma interaction with the lossy-dielectric media represented by the tissue results in surface charging. Poisson's equation is solved throughout the computational domain, including the gas phase and the solid tissue.

The model used in the investigation is *nonPDPSIM*. The gas phase reaction mechanism and algorithms are the same as those described in [44] and hence will be only briefly described here. *nonPDPSIM* is a two-dimensional simulation in which Poisson's equation for the electric potential, and transport equations for charged and neutral species are solved. The electron temperature, T_e, is obtained by solving an electron energy conservation equation with transport and rate coefficients coming from local solutions of Boltzmann's equation. Radiation transport and photoionization are included by implementing a Green's function propagator.

The model geometry, shown in figure 1(*b*), mimics that of the experiments of Fridman *et al* [10]. A DBD is positioned a few millimetres above a thumb having a curved surface with respect to the plasma applicator. The top boundary of the computational domain is the powered metal electrode of the DBD. The electrode is covered by a dielectric 0.8 mm thick having dielectric constant $\varepsilon/\varepsilon_0 = 4$. The other bounding surfaces of the computational domain are grounded. Ideally, these boundaries should be extended as far as possible from the thumb for the proper representation of a floating dielectric electrode. In our geometry, the ground planes are closer for computational convenience: 1.5 mm to the left of the tip of the thumb and 1 mm below the bottom surface (nail) of the thumb. Also, for computational convenience, the thumb was terminated approximately where shown on the right side of figure 1(*b*), and the ground plane is 1 mm beyond the termination. Hence the thumb is not in direct physical contact with electrical ground.

The numerical grid uses an unstructured mesh with triangular elements and refinement regions to resolve the details of the plasma filaments, cell interior and nuclei. The mesh consists of approximately 13 000 nodes, of which about 4000 are in the plasma region to resolve plasma filaments and the majority of the remainder are expended in resolving the cellular structure. The gas mixture is atmospheric pressure dry air, $N_2/O_2 = 80/20$. For the cases discussed here, the mean free path of ionizing photons was 100 μm. To initiate the discharge, seed electron currents were injected from the upper dielectric surface. The streamer was then sustained at the dielectric–gas interface by the naturally occurring secondary electron currents due to ion bombardment (secondary electron emission coefficient $\gamma = 0.15$) and VUV photon illumination ($\gamma = 0.01$).

A DBD filamentary discharge is produced between the DBD applicator and the surface of the thumb, 1–2 mm away. The plasma transport equations are solved outside the thumb. Inside the thumb, a conductivity, σ, and dielectric permittivity, $\varepsilon/\varepsilon_0$, are specified for different thumb regions and different cell structures. Charge densities inside the tissue for use in Poisson's equation are obtained by integrating $\partial\rho/\partial t = -\nabla\cdot\vec{j} = -\nabla\cdot\sigma\vec{E}$. Charge naturally accumulates at interfaces between more and less conductive structures, such as at the cytoplasm–membrane interface as well as on the cytoplasm–nucleoplasm interface. We do not specify boundary conditions for electric fields between cells in the skin and between the cell and nuclei. We solve for electric potential throughout the computational domain. Each computational node is assigned the properties of specific material (cytoplasm, membranes, dead cells) with appropriate permittivities and conductivities. Solution of Poisson's equation in concert with charge transport naturally provides the appropriate continuity of electric fields across boundaries in the presence of charges.

We attempted to resolve the cellular structure of the surface layers of the skin to a sufficient level of detail to resolve intercellular currents, interactions between cells and the influence of different cells shapes and types of different tissue. This would be prohibitively computationally expensive over the entire thumb. Hence we resolved the cellular structure

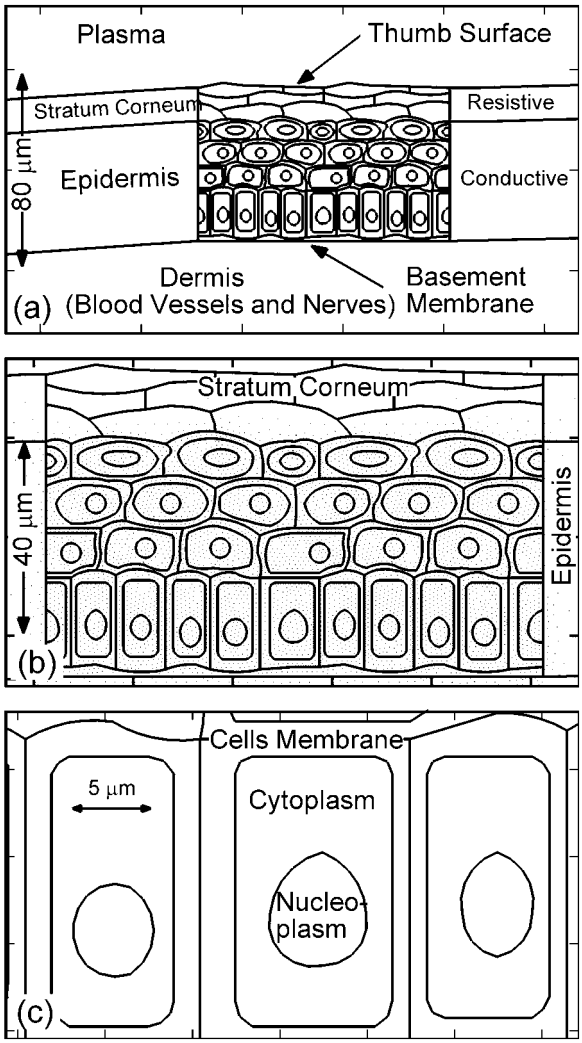

Figure 2. Representation of skin in the model. (*a*) Overall structure of cells in the mesh including the outer epidermal layer (stratum corneum) which is highly resistive, layers of epidermal cells with nuclei and the dermis. The structures in the dermis are not resolved in the model. Outside the central region of the epidermis, cells are not resolved and only average electrical properties are used. (*b*) Enlargement of the epidermis showing the ensemble of cells in the unstructured mesh. (*c*) Typical cells' elements and dimensions. Membranes were made thicker than their real dimensions in order to resolve their interiors.

in a small patch approximately 100 μm wide and 80 μm deep, as shown in figure 2. This patch was located at the site at which a plasma filament strikes the skin. Average tissue values for conductivity and permittivity were used elsewhere.

Our representation of mammalian skin consisted of two components [45]. The first is a thin outer layer, the epidermis, which includes the electrically resistive stratum corneum, and a thicker, collagenous, inner layer called the dermis. The epidermis was resolved on a cellular basis. The epidermis is irregular and heterogeneous, which we attempted to resolve, and is punctuated by many sweat glands and hair follicles, which we did not include. The epidermis is a self-renewing structure by virtue of division by the innermost layer of cells. As a result, the cells closest to the surface are the 'oldest', and have more compact shapes and resistive electrical properties. Lipid bilayers (two thin layers of mainly phospholipids molecules) are the core structure of cell membranes which are 5–10 nm wide.

The electrical properties of skin are largely determined by the stratum corneum which has a thickness of the order 15 μm and consists of layers of dead cells. We reproduced the epidermis layer with the layer of dead cells, a layer of horizontal cells and basement cells. The membranes are made thicker than in reality in order to resolve their interiors. The fine details of the intracellular structures were not resolved beyond a single nucleus immersed in cytoplasm, as shown in figure 2(*c*).

The nature of the interaction of electric fields with tissue is determined by the dielectric properties of the biological material. The values available in the literature for dielectric constants, ε, and conductivities of cell membranes, cytoplasm, nuclear membranes and nucleoplasm vary over large ranges. The values we used here were measured using dielectric spectroscopy [46, 47]. The ranges of cell parameters from different experimental studies are given in table 1, where lower and upper experimental limits are shown, with recommended reference parameters given in parentheses. Typical values for $\varepsilon/\varepsilon_0$ for the plasma membrane of mammalian cells are about 6, and σ is about $10^{-7}\,\Omega^{-1}\,\mathrm{cm}^{-1}$. For the cytoplasm, ε is between 30 and that of water, 80, and σ is typically one-fifth that of seawater, $0.005\,\Omega^{-1}\,\mathrm{cm}^{-1}$.

The base case values of permittivities and conductivities used in the model are shown in table 2 with the corresponding values of τ. We adopted recommended values for cell parameters, except for the dielectric constants for cytoplasm and the nuclear envelope where lower limits were used. For example, we used $\varepsilon/\varepsilon_0 = 30$ for cytoplasm and $\varepsilon/\varepsilon_0 = 20$ for the nuclear envelope thereby keeping the recommended ratio of 3 to 2. This choice of lower limits for $\varepsilon/\varepsilon_0$ was connected with limitations of the computational time step which, in its turn, is determined by the dielectric relaxation time. We do not resolve the internal features of nuclei. Instead, the nuclei are assumed to be one material with properties of the nuclear envelope.

We note that our model is two-dimensional whereas the interaction of multiple-circular filaments strictly requires a three-dimensional simulation. We expect the results discussed below on the interaction of these filaments with tissue will have some dependence on dimensionality; however, the trends are likely not significantly sensitive to dimensionality.

4. Propagation of plasma filaments and interaction with skin

The experimental device we modelled is patterned after the DBD of Fridman *et al* [10]. The powered electrode is covered by a dielectric and the second electrode is human skin. In the model, the voltage pulse has a rise-time of 0.1 ns and an amplitude of -30 kV for the base case. Initially, three simultaneously propagating filaments were modelled without considering the cellular structure in the mesh to investigate the variability and interaction of the filaments due to the non-uniform surface presented by the thumb. More detailed studies

Table 1. Range of cell parameters in the double-shell model. Recommended values are noted in parentheses [32, 46, 47].

	Dead cells	Cell membrane	Cytoplasm	Nuclear envelope	Nucleoplasm
$\varepsilon/\varepsilon_0$	2.1–80	1.4–16.8 (5.8)	30–77 (60)	6.8–100 (41)	32–300 (120)
σ (Ω^{-1} cm^{-1})	10^{-6}–10^{-8}	8×10^{-10}–6×10^{-7} (8.7×10^{-8})	3×10^{-4}–1×10^{-2} (4.8×10^{-3})	8×10^{-7}–7×10^{-5} (3.0×10^{-5})	3×10^{-3}–22×10^{-3} (9.5×10^{-3})

Table 2. Permittivities and conductivities used in the model and dielectric relaxation times.

	Dead cells	Cell membrane	Cytoplasm	Nuclear envelope	Nucleoplasm
$\varepsilon/\varepsilon_0$	3	5.8	30	20	—
σ (Ω^{-1} cm^{-1})	10^{-8}	8.7×10^{-8}	4.8×10^{-3}	3.0×10^{-5}	—
τ (s)	2.7×10^{-5}	5.9×10^{-6}	5.5×10^{-10}	5.9×10^{-8}	—

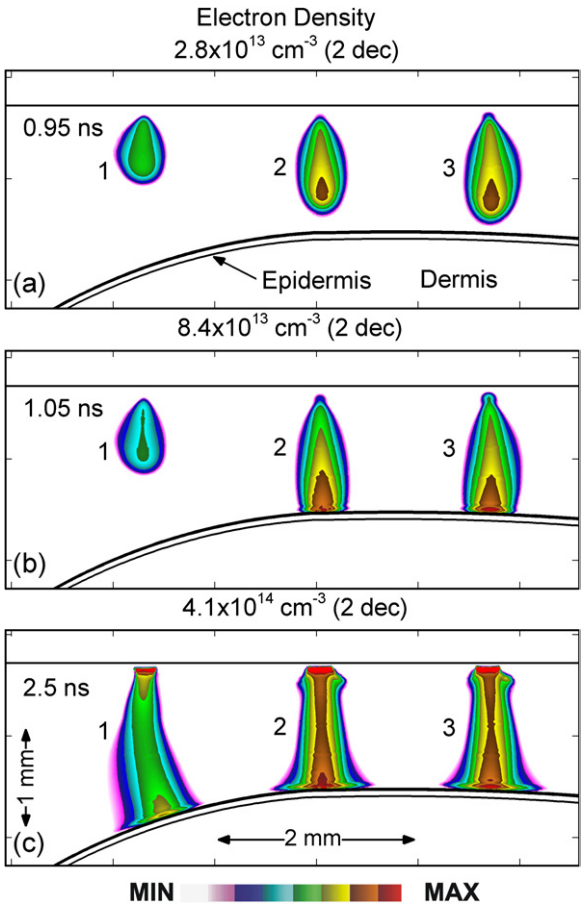

Figure 3. Electron density for three filaments at times of (*a*) 0.95 ns, (*b*) 1.05 ns and (*c*) 2.5 ns. The conditions are atmospheric pressure air, −30 kV applied voltage and simultaneous production of initiating secondary emission from the dielectric for the three filaments.

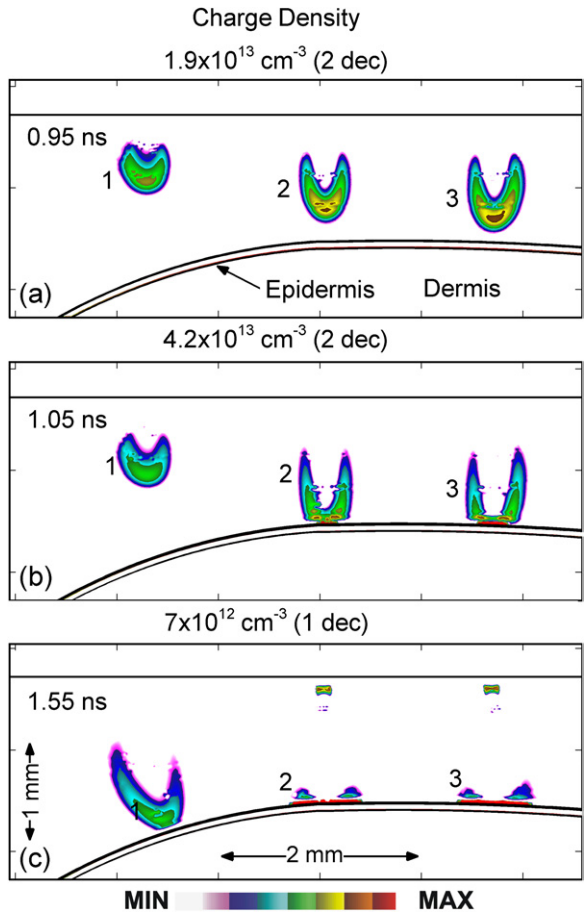

Figure 4. Negative space charge for three filaments for the conditions of figure 3 at times of (*a*) 0.95 ns, (*b*) 1.05 ns and (*c*) 1.55 ns. Charges accumulate on the surface of the skin. Individual filaments compete for the available surface area of the dielectric to deposit their charge.

of the cellular response to the plasma filaments were performed while modelling a single filament.

Plasma parameters for discharges with three simultaneous or one single filament are shown in figures 3–7. The electron density, charge density and electron source function for the three filaments are shown in figures 3–5. The notation 'dec' in these and following figures indicates the number of decades of dynamic range plotted. The electron temperature, T_e, electric field, electron density and charge density for a single filament near the thumb surface are shown in figures 6 and 7. The thumb serves as the counter electrode and hence limits the discharge current in a manner similar to that of a conventional DBD. The microdischarges are characterized by high electron densities (4×10^{14} cm^{-3}) and high electron temperatures, up to 8.2 eV, in the heads of the streamers, as shown in figures 3 and 7(*a*). The width of the resulting ionized channel is about 300–500 μm, values typical for negative filaments. The power dissipated in the column of a single filament is about 12 kW cm^{-3} or about 0.75 W for the duration of the filament. For filament durations

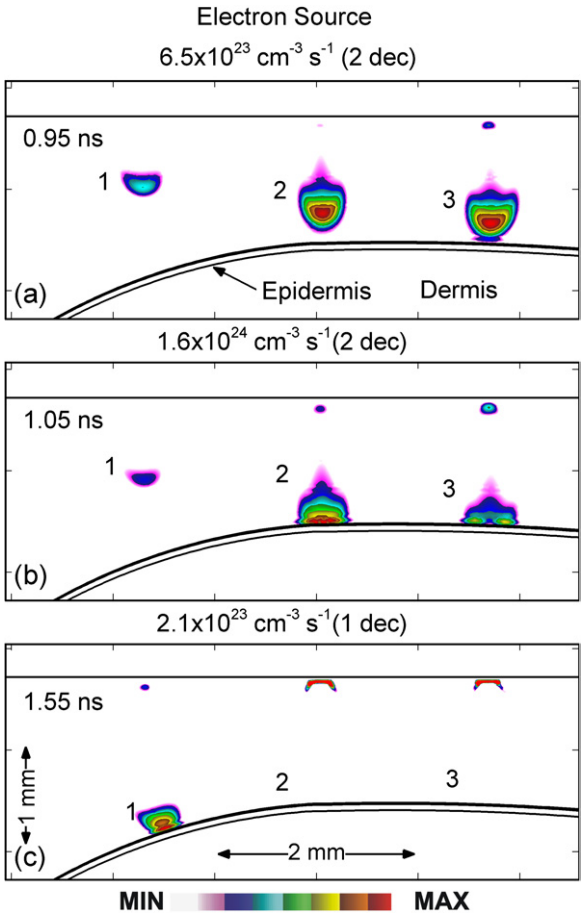

Figure 5. Electron impact sources for three transient filaments for the conditions of figure 3 at times of (*a*) 0.95 ns, (*b*) 1.05 ns and (*c*) 1.55 ns.

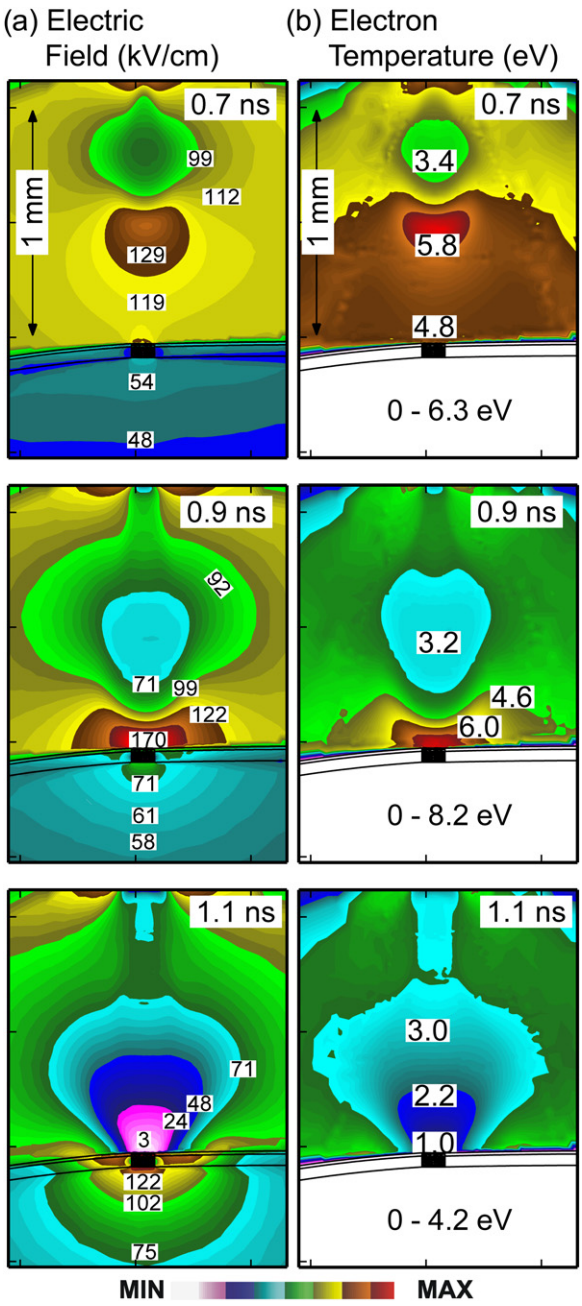

Figure 6. Electrical properties at the surface of the skin upon intersection of a single filament (location of filament 2) at times of 0.7, 0.9 and 1.1 ns. (*a*) Electric field and (*b*) electron temperature. The electric field reaches 170 kV cm^{-1} near the thumb surface and penetrates deeply inside the tissue, more than 1 mm. Electric fields in excess of 100 kV cm^{-1} penetrate below the epidermis.

of up to about 5 ns, filament area densities of about 100 cm^{-2} and a repetition rate of 10 kHz, the total dissipated power is about 4 mW cm^{-2}.

The differences in the shapes, plasma densities and electric fields produced by the three streamers are determined by the distance between the dielectric and skin, and the surface normal of the skin relative to the dielectric. For example, the gap distance and orientation of the skin are nearly the same for filaments 2 and 3, and hence their plasma densities are similar, although the propagation speed of filament 3 is marginally higher than that of the middle filament. The gap distance is larger and orientation of the skin more skewed for filament 1, as shown in figure 3. The path of filament 1 begins as being relatively vertical and parallel to filaments 2 and 3. The filament reorients itself towards the perpendicular to the thumb surface about 0.5 mm above the surface. This path is indicated by the charge density and ionization source which tracks the progress of the head of the streamer. The end result is a plasma channel that follows a curved path to ultimately orient itself perpendicular to the skin. There is also some evidence for electrostatic repulsion between two closely spaced negative filaments, an effect observed by Luque and Ebert [48].

After intersecting the skin, electrons from filaments 2 and 3 spread along the surface of the skin. Individual filaments compete for the available surface area of the dielectric to deposit their charge. As a result of the surface charging, the axial electric field is locally reduced and components of the electric field along the surface are produced [49, 50]. With the charging of the skin, the voltage drop across the gap decreases as in a conventional DBD. As a result, the velocity of filament 1 decreases as well. It takes 1.6 ns for filament 3 to reach the surface of the thumb surface compared with 1 ns for filaments 2 and 3, an effect not attributable to only the difference in path length.

The maximum electric field in the streamer head prior to reaching the skin is 120–140 kV cm^{-1}, as shown in figure 6. As

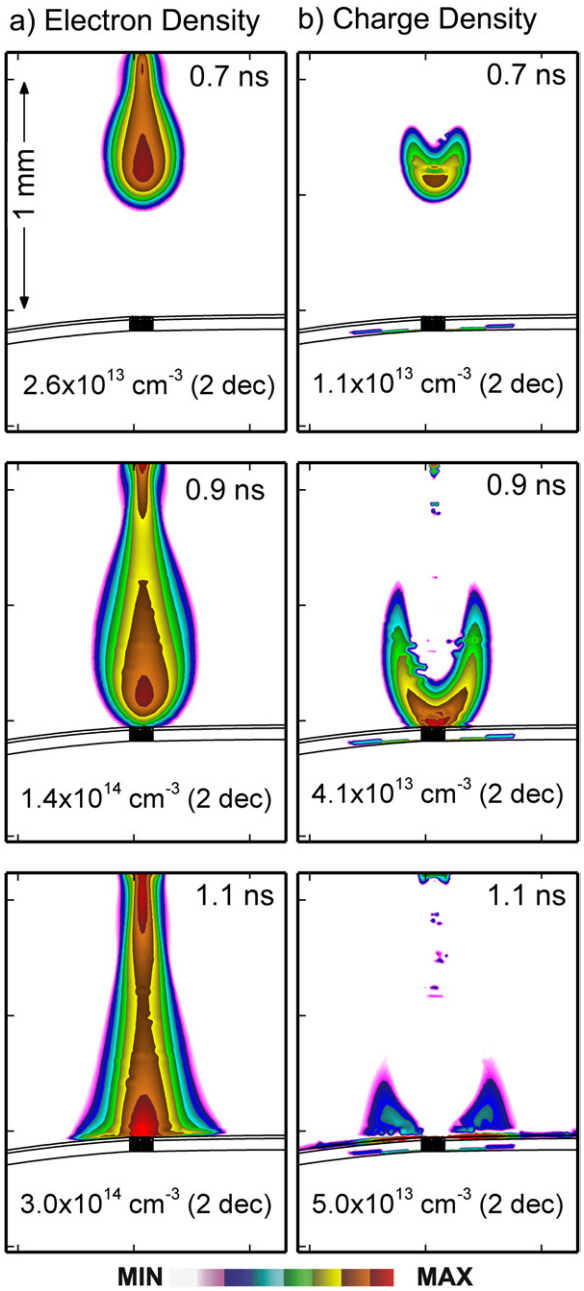

Figure 7. Plasma properties at the surface of the skin upon intersection of a single filament (location of filament 2) at times of 0.7, 0.9 and 1.1 ns. (*a*) Electron density and (*b*) negative charge density. Notice the spreading of the discharge along the surface of the skin after the filament intersects the thumb surface, similar to conventional DBDs.

the conductive channel forms behind the head of the streamer, more voltage is compressed in front of the streamer, thereby increasing the electric field in the head of the streamer. When the streamer intersects the skin (the opposing dielectric to the powered electrode), the gap is closed by a conductive channel and charging of the skin is rapid. This produces electric fields of 170–200 kV on the surface of the skin. The electric fields penetrating into the skin prior to and after the arrival of the plasma produce conduction and displacement currents in the tissue. The conduction currents move charges in the cells which accumulate at the interfaces between more and less conductive regions.

5. Intracellular charging and electric fields

Recall that the dielectric relaxation times of cellular structures, $\tau = \varepsilon/\sigma$, determine the importance of the capacitive or resistive component of the membrane and cytoplasm with respect to the duration of a voltage pulse. For pulse durations that are long compared with τ, the resistive component dominates. For pulse durations that are short compared with τ, the capacitive component dominates. The duration of the DBD discharge pulse and its major interaction with the tissue is a few nanoseconds, which is short compared with τ of the membrane (5.9 μs), and comparable to that of the cytoplasm (0.5 ns).

The accumulation of positive and negative charges on cell membranes and nuclei is shown in figures 8 and 9 for times when the plasma filament is half the way from the thumb surface (0.7 ns), the filament just touches the surface (0.9 ns) and after the gap is closed by the plasma channel and the surface of the skin charges (1.1 ns). These times correspond to the position of the filament shown in figures 6 and 7. Positive and negative charges accumulate on opposite sides of cell membranes and nuclei. The maximum charge densities are approximately 10^{15} cm^{-3} or (1–2) $\times$ 10^{-4} C cm^{-3}. Although these charge densities are large, they are consistent with the conductivities for mammalian cells cited in the literature [46, 47] and the charge buildup across cell membranes required to produce potential differences of up to a few volts. The initial charging of the cells occurs during the voltage rise-time (0.1 ns) when displacement currents intersect the skin and induce conduction currents through the cells. The displacement and conduction currents then increases as the filament approaches the surface and the approaching electric fields increase by virtue of the voltage compression ahead of the filament.

The charges on the cell membranes are not saturated as the dielectric relaxation time of the membranes is much longer than the lifetime of the filament (1–2 ns). Note the accumulated positive charge on the basement membrane and negative charges on the surface of the thumb at 1.1 ns when the filament arrives at the surface (figures 8(*c*) and 9(*c*)). The corresponding electric fields are shown in figure 10 for the same time sequence, with an enlargement of two latter times in figure 11. During propagation of the filament and prior to striking the surface, the electric fields in the cell interiors are not high, $<$13 kV cm^{-1}. These electric fields do not significantly change until the filaments approach and touch the surface. The largest potential drop across a cell structure and, as a result, the highest electric field occurs in the stratum corneum layer as this layer is the most resistive. Note also the high values of electric field in fairly conductive parts of the cell–cell cytoplasm, on the order of 35 kV cm^{-1}. This indicates that electric fields produced by filamentary DBDs can penetrate the cells and may produce similar effects as tailored pulsed electric fields [29–31].

Electric fields and charge accumulation are shown in figure 12 for a chord cutting across a number of cells. The

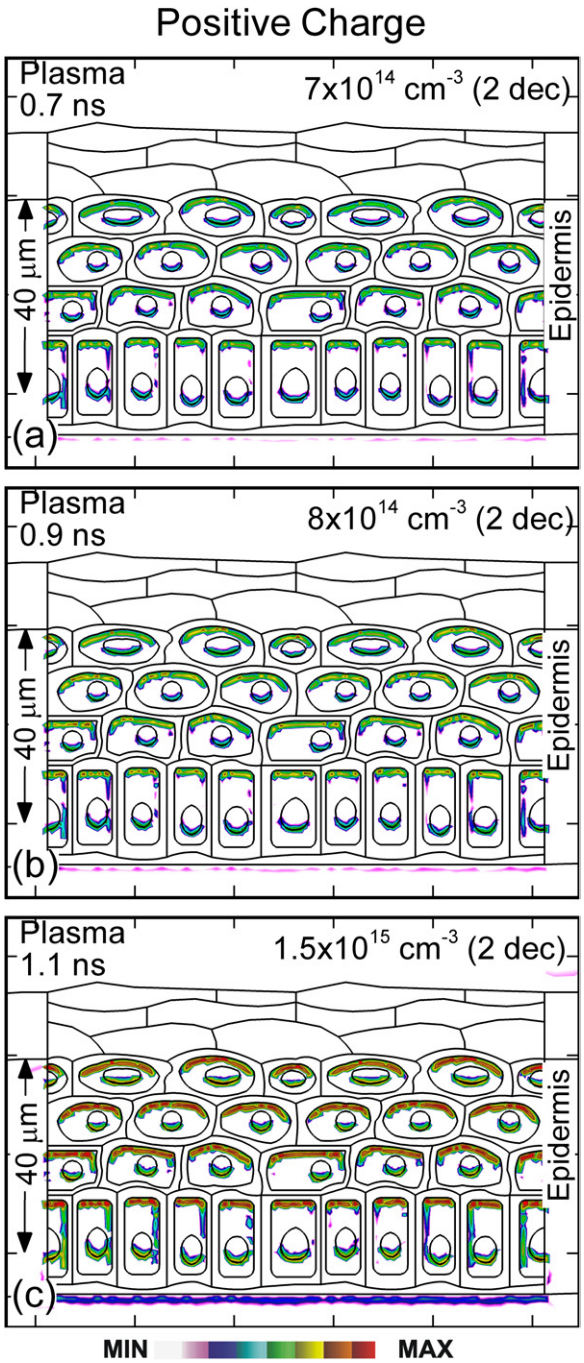

Figure 8. Positive charge accumulation on cell membranes and nuclei. The three frames correspond to when the filament is (*a*) in the middle of the gap (0.7 ns), (*b*) first touching the surface (0.9 ns) and (*c*) when the electric field of the filament penetrates into the thumb (1.1 ns).

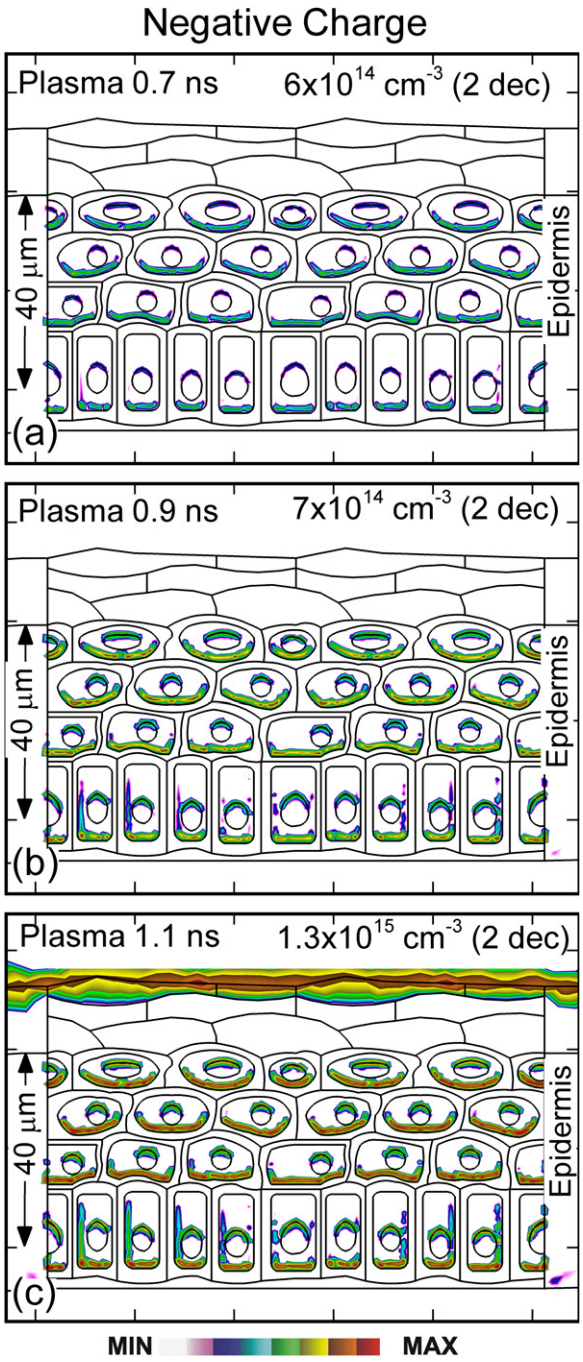

Figure 9. Negative charge accumulation on cell membranes and nuclei. The three frames correspond to when the filament is (*a*) in the middle of the gap (0.7 ns), (*b*) first touching the surface (0.9 ns) and (*c*) when the electric field of the filament penetrates into the thumb (1.1 ns).

electric fields across the membrane are highest (150 kV cm^{-1}) when the filament touches the thumb surface (1.1 ns). The voltage drop recalculated for the thickness of an actual lipid membrane (5–10 nm) is about 0.1 V, a value corresponding to the lower limit of cell electroporation for long pulses. However, as DBDs consist of numerous filaments, the accumulative effect of multiple filaments may initialize electroporation. The positive and negative charges are symmetrically distributed on the cell membranes and nuclei, as shown in figure 12(*c*). That is not necessarily the general case as a filament can arrive at the surface at some distance from this particular cell, thereby producing charges on the side walls of membranes. During the charging time of the outer membrane, potential differences are also generated across sub-cellular membranes. Due to their lower conductivity, cell organelles (nuclei) experience large electric fields reaching 43–47 kV cm^{-1}. During the short life-times of these filaments, the dielectric properties of cell structures determine the electric field distribution as opposed to their resistivity.

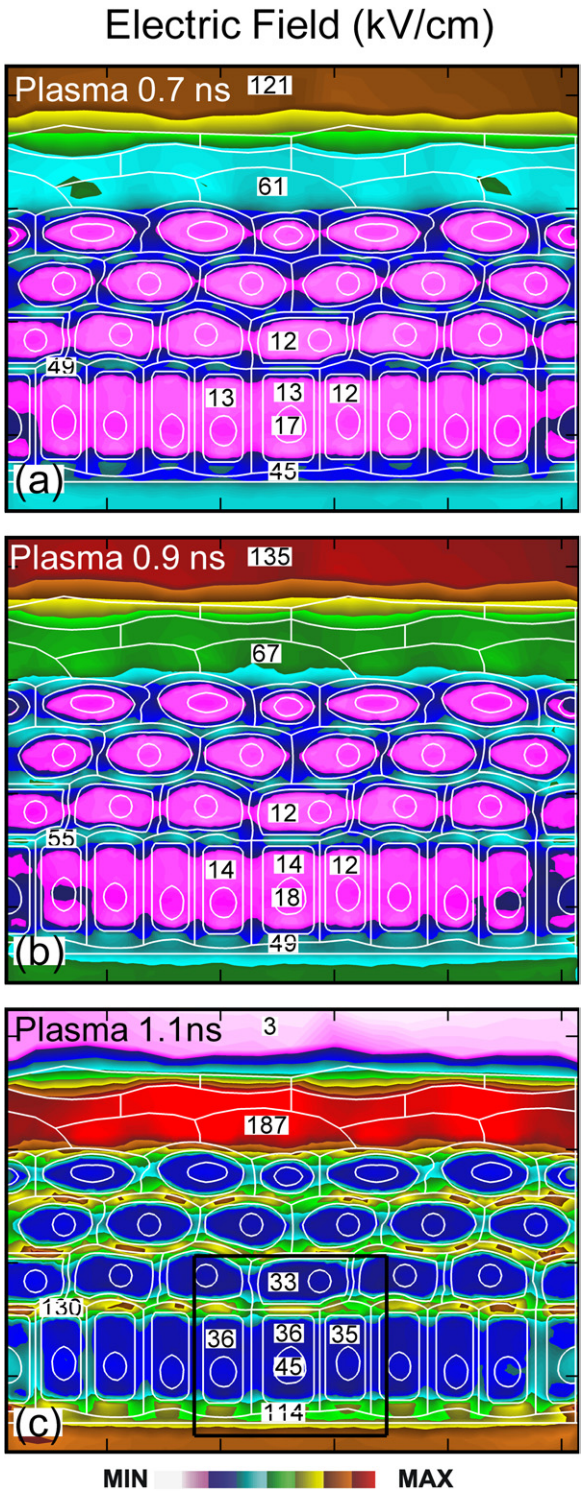

Figure 10. Electric fields inside the epidermal layer at times of (*a*) 0.7 ns, (*b*) 0.9 ns and (*c*) 1.1 ns corresponding to figures 8 and 9. Prior to the filament striking the surface, the intracellular electric fields are determined by displacement currents from the filament. These fields do not significantly change until after the filament approaches the surface. The largest potential drop and, as a result, the highest electric field is in the resistive stratum corneum layer.

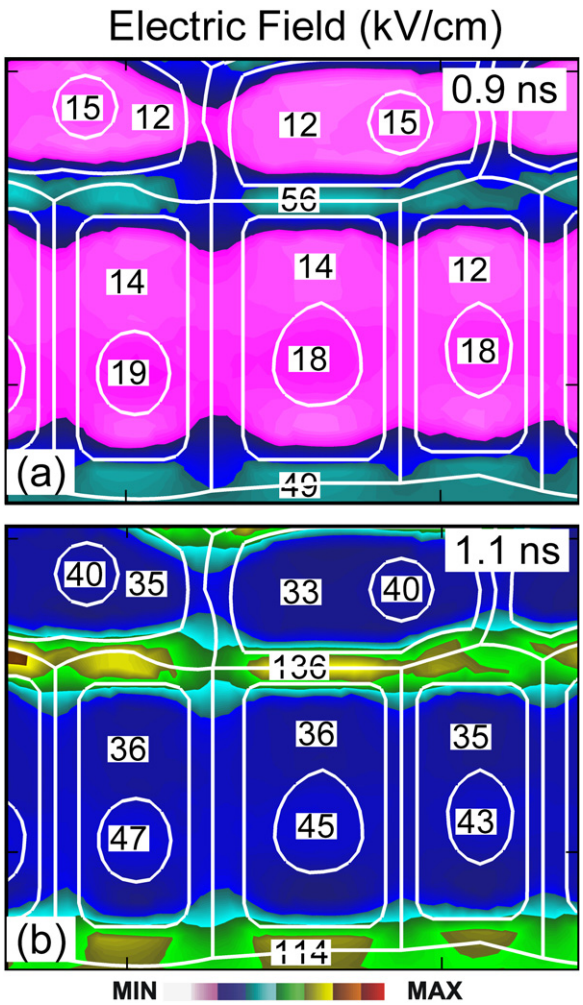

Figure 11. Electric fields on the cellular scale for the conditions of figure 10 at times of (*a*) 0.9 ns and (*b*) 1.1 ns.

The dependence of the electric fields across the cell as a function of membrane permittivity and applied voltage is shown in figure 13. The membrane permittivity was increased from the reference value of 5.8 to the upper recommended limit of 16.8. (See table 1.) This increase in dielectric constant by a factor of 3 resulted in a decrease in the electric field across the membranes by 40%. Increasing the applied voltage to the DBD applicator by a factor of 1.66 (from 30 to 50 kV) resulted in an increase in electric field by a factor of 1.5 to nearly 200 kV cm^{-1}. This is a regime in which electroporation becomes more probable. Note that the induced electric fields do not scale absolutely linearly with applied voltage in large part because the charging of the surface of the skin, and the lateral spreading of that change, does not scale absolutely linearly with voltage.

The power of the filaments can be increased by increasing the permittivity of the dielectric to increase its capacitance. Although exhaustive studies have not been performed, based on prior studies we have found that the charging properties of the surface at the location where the filament strikes are not sensitive functions of the dielectric capacitance. With more capacitance, there is more spreading of the discharge along the surface, in this case, of the skin. As such, electric fields will be produced in and over a larger extent of tissue.

Our choice of voltage rise-time is short compared with most experiments, and was chosen for computational

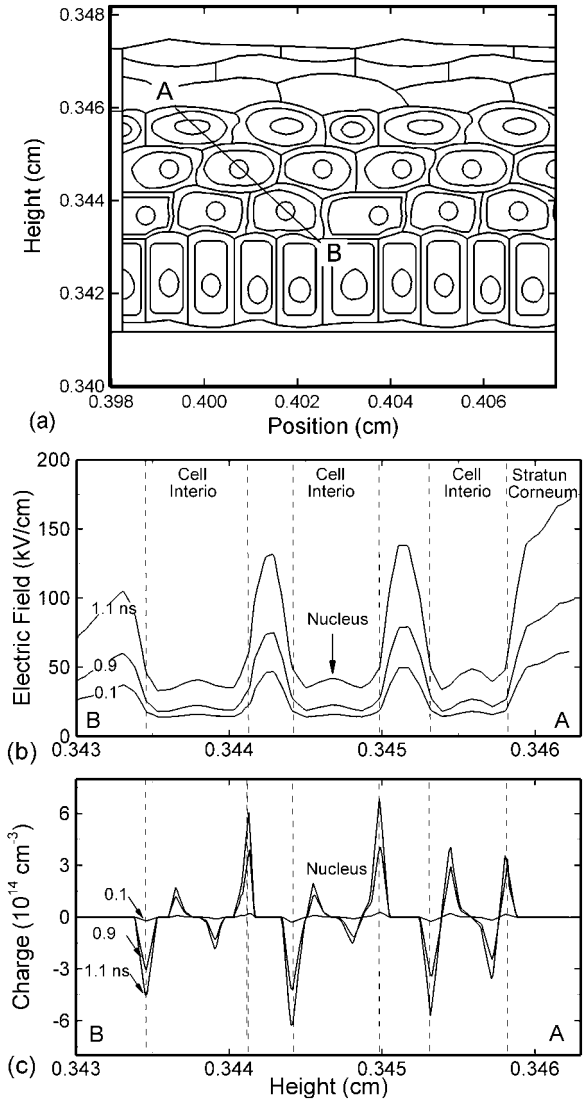

Figure 12. Electric field and charge densities inside the cells along a chord (in the direction of increasing height). (*a*) Outline of cells and chord along which the profiles are shown. (*b*) Electric fields along the chord produced by displacement currents from the filament (0.1 ns), when the filament approaches the surface (0.9 ns) and when the filament interacts with the surface (1.1 ns). The electric field is highest (150 kV cm^{-1}) when the filament touches the thumb surface (1.1 ns). (*c*) Charge densities along the chord. The charges are symmetrically distributed across membranes and nuclei.

convenience. In related studies, we found that fast rising voltage pulses allow an overshoot of the breakdown voltage, and hence higher filament propagation speeds, but otherwise do not significantly affect the properties of an individual streamer. The displacement currents at the beginning of the pulse through the tissue are larger due to the shorter rise-time. However, the electric fields produced within the tissue by these initial transients are small compared with those produced by the arrival of the filament at the surface of the tissue. In experimental studies by Ayan *et al*, fast rising pulses (e.g., 1–3 kV ns^{-1}) were found to produce more uniform arrays of filaments that are less likely to form micro-arcs [51, 52]. Fast rising pulses are therefore potentially safer for therapeutic purposes.

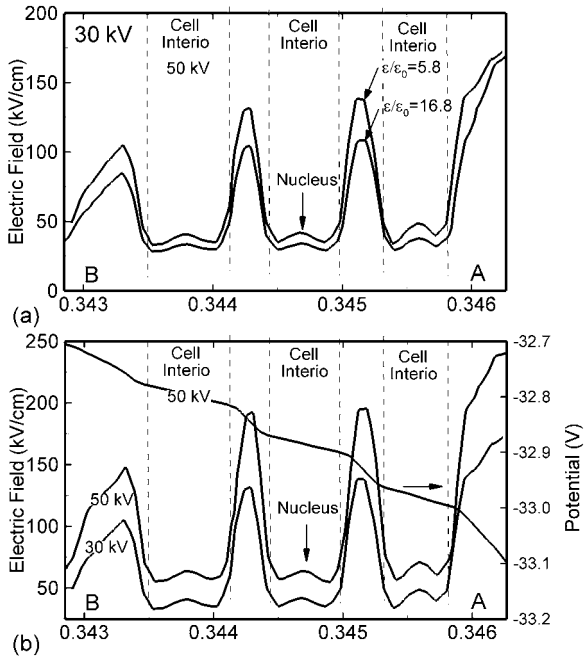

Figure 13. Electric fields for different operating parameters and cell properties. (*a*) Electric fields for membrane dielectric constants of 5.8 and 16.8 and (*b*) electric fields for −30 and −50 kV on the applicator. The increase in dielectric constant by a factor of 3 results in a decrease in electric field across the membranes by 40%. The increase in applied voltage by a factor of 1.66 results in a commensurate increase in electric field.

6. Concluding remarks

The electrical properties of negative filaments in a DBD intersecting with human skin were computationally investigated. The typical life-times of filaments and the intersection of the head of the filaments with the skin are shorter than or comparable to the dielectric relaxation times of cell components. As a result, there can be significant electric field penetration into intracellular structures. Trans-membrane potentials in excess of 0.1 V, approaching the regime of electroporation, can be produced for conditions typically used for DBD plasma treatment of tissue. The potential use of DBDs for electric field therapy or electroporation will in part be determined by reproducibility. We found that adjacent filaments in a DBD can have different propagation properties determined, in part, by the curvature of the tissue being treated and small variations in the slope of the DBD applicator compared with the skin. Since the intracellular generation of electric fields ultimately depends on the rate of voltage rise and charging as the filament intersects the skin, processes such as electroporation may result from ensemble averages of the contributions of many individual filaments. To the degree there is a threshold for these processes, only a subset of the filaments may produce intracellular electric fields that breach the threshold.

In actual operation of DBDs for therapeutic purposes, it is likely that the air would be humid, and hence contain water vapour. Aside from radical generation, which would certainly impact plasma chemical interactions with tissue, we found from prior studies that there will not be significant changes

in the interaction of DBD filaments with skin provided that the skin itself is not wetted. For example, the E/N at which net ionization occurs in air with 2% water vapour compared with dry air increases by a few Townsends (172 Td compared with 175 Td). Hence it is not likely that significantly different discharge conditions will be required to achieve the same tissue interactions with small amounts of humidity.

Acknowledgment

This work was supported by the US Department of Energy Office of Fusion Energy Science Contract DE-SC0001939.

References

[1] Dobrynin D, Fridman G, Friedman G and Fridman A 2009 Physical and biological mechanisms of direct plasma interaction with living tissue *New J. Phys.* **11** 115020
[2] Kong M G, Kroesen G, Morfill G, Nosenko T, Shimizu T, van Dijk J and Zimmermann J L 2009 Plasma medicine: an introductory review *New J. Phys.* **11** 115012
[3] Boudam M K, Moisan M, Saoudi B, Popovici C, Gherardi N and Massines F 2006 Bacterial spore inactivation by atmospheric-pressure plasmas in the presence or absence of UV photons as obtained with the same gas mixture *J. Phys. D: Appl Phys.* **39** 3494
[4] Laroussi M 2009 Low-temperature plasmas for medicine *IEEE Trans. Plasma Sci.* **37** 714
[5] Deilmann M, Halfmann H, Bibinov N, Wunderlich J and Awakowicz P 2008 Low-pressure microwave plasma sterilization of polyethylene terephthalate bottles *J. Food Prot.* **71** 2119
[6] Stoffels E, Sakiyama Y and Graves D 2008 Cold atmospheric plasma: charged species and their interactions with cells and tissues *IEEE Trans. Plasma Sci.* **36** 1441
[7] Kieft I E, Kurdi M and Stoffels E 2006 Reattachment and apoptosis after plasma-needle treatment of cultured cells *IEEE Trans. Plasma Sci.* **34** 1331
[8] Kieft I E, Darios D, Roks A J M and Stoffels-Adamowicz E 2005 Plasma treatment of mammalian vascular cells: a quantitative description *IEEE Trans. Plasma Sci.* **33** 771
[9] Fridman G, Brooks A D, Balasubramanian M, Fridman A, Gutsol A, Vasilets V N, Ayan H and Friedman G 2007 Comparison of direct and indirect effects of non-thermal atmospheric pressure plasma on bacteria *Plasma Process. Polym.* **4** 370
[10] Fridman G, Peddinghaus M, Ayan H, Fridman A, Balasubramanian M, Gutsol A, Brooks A and Friedman G 2006 Blood coagulation and living tissue sterilization by floating electrode dielectric barrier discharge in air *Plasma Chem. Plasma Process.* **26** 425
[11] Kalghatgi S U *et al* 2007 Mechanism of blood coagulation by non-thermal atmospheric pressure dielectric barrier discharge plasma *IEEE Trans. Plasma Sci.* **35** 1559
[12] Fridman G, Shereshevsky A, Jost M M, Brooks A D, Fridman A, Gutsol A, Vasilets V and Friedman G 2007 Floating electrode dielectric barrier discharge plasma in air promoting apoptotic behavior in melanoma skin cancer cell lines *Plasma Chem. Plasma Process.* **27** 163
[13] Fridman G, Friedman G, Gutsol A, Shekhter A B, Vasilets V N and Fridman A 2008 Applied plasma medicine *Plasma Process. Polym.* **5** 503
[14] Lee S M, Hong Y J, Seo Y S, Iza F, Kim G Ch and Lee J K 2009 Simulations of biomedical atmospheric-pressure discharges *Comput. Phys. Commun.* **180** 636
[15] Kim G C, Kim G J, Park S R, Jeon S M, Seo H J, Iza F and Lee J K 2009 Air plasma coupled with antibody-conjugated nanoparticles: a new weapon against cancer *J. Phys. D: Appl. Phys.* **42** 032005
[16] Sladek R E J and Stoffels E 2005 Deactivation of *Escherichia coli* by the plasma needle *J. Phys. D. Appl. Phys.* **38** 1716
[17] Goree J, Liu B, Drake D and Stoffels E 2006 Killing of *S. mutans* bacteria using a plasma needle at atmospheric pressure *IEEE Trans. Plasma Sci.* **34** 1317
[18] Tuemmel S, Mertens N, Wang J and Vioel W 2007 Low temperature plasma treatment of living human cells *Plasma Process. Polym.* **4** S465
[19] Kuchenbecker M, Bibinov N, Kaemlimg A, Wandke D, Awakowicz P and Viol W 2009 Characterization of DBD plasma source for biomedical applications *J. Phys. D: Appl. Phys.* **42** 045212
[20] Rajasekaran P, Mertmann P, Bibinov N, Wandke D, Viol W and Awakowicz P 2009 DBD plasma source operated in single-filamentary mode for therapeutic use in dermatology *J. Phys. D: Appl. Phys.* **42** 225201
[21] Kaemling C, Kaemling A, Tummel S and Vioel W 2005 Plasma treatment on finger nails prior to coating with a varnish *Surf. Coat. Technol.* **200** 668
[22] Shekhter A B, Serezhenkov V A, Rudenko T G, Pekshev A V and Vanin A F 2005 Beneficial effect of gaseous nitric oxide on the healing of skin wounds *Nitric oxide: Biol. Chem.* **12** 210
[23] Schaffer M R, Tantry U and Barbul A 1997 Nitric oxide metabolism in wounds *J. Surg. Res.* **71** 25
[24] Sweet F, Kao M S, Lee S C, Hagar W L and Sweet W E 1980 Ozone selectively inhibits growth of human cancer cells *Science* **209** 931
[25] Weaver J C 2000 *Electroporation of Cells and Tissues* (Boca Raton, FL: CRC Press)
[26] Barnett A and Weaver J C 1991 Electroporation: a unified, quantitative theory of reversible electrical breakdown and mechanical rupture in artificial planar bilayer membranes *Bioelectrochem. Bioenergetics* **25** 163–82
[27] Weaver J C 2003 Electroporation of biological membranes from multicellular to nano scales *IEEE Trans. Dielectr. Electr. Insul.* **10** 754
[28] Weaver J C and Chizmadzhev Yu A 1996 Theory of electroporation: a review *Bioelectrochem. Bioenergetics* **41** 135
[29] Schoenbach K H, Beebe S J and Buescher E S 2001 Intracellular effect of ultrashort electrical pulses *J. Bioelectromagn.* **22** 440
[30] Beebe S J, Fox P M, Rec L J, Somers K, Stark R H and Schoenbach K H 2002 Nanosecond pulsed electric field (nsPEF) effects on cells and tissues: apoptosis induction and tumor growth inhibition *IEEE Trans. Plasma Sci.* **30** 286
[31] Buescher E S and Schoenbach K H 2003 The effects of submicrosecond, high intensity pulsed electric fields on living cells—intracellular electromanipulation *IEEE Trans. Dielectr. Electr. Insul.* **10** 788
[32] Chizmadzhev Yu A, Zarnitsin V G, Weaver J C and Potts R O 1995 Mechanism of electroinduced ionic species transport through a multilamellar lipid systems *Biophys. J.* **68** 749
[33] Neu J C and Krassowska W 1999 Asymptotic model of electroporation *Phys. Rev.* E **59** 3471
[34] Stewart D A, Gowrishankar T R and Weaver J C 2004 Transport lattice approach to describing cell electroporation: use of a local asymptotic model *IEEE Transa. Plasma Sci.* **32** 1696
[35] Stewart D A, Gowrishankar T R, Smith K C and Weaver J C 2005 Cylindrical cell membranes in uniform applied electric fields: validation of a transport lattice method *IEEE Trans. Biomed. Eng.* **52** 1643

[36] Hu Q, Viswanadham S, Joshi R P, Schoenbach K H, Beebe S J and Blackmore P F 2005 Simulations of transient membrane behavior in cells subjected to a high-intensity ultrashort electric pulse *Phys. Rev.* E **71** 031914
[37] Hu Q, Joshi R P and Schoenbach K H 2005 Simulations of nanopore formation and phosphatidylserine externalization in lipid membranes subjected to a high intensity, ultrashort electric pulse *Phys. Rev.* E **72** 031902
[38] Cascales J J L, de la Torre J G, Marrink S J and Berendsen H J C 1996 Molecular dynamics simulation of a charged biological membrane *J. Chem. Phys.* **104** 2713
[39] Tarek M 2005 Membrane electroporation: a molecular dynamics simulation *Biophys. J.* **88** 4045
[40] Timoshkin I V, MacGregor S J, Fouracre R A, Crichton B H and Anderson J G 2006 Transient electrical field across cellular membranes: pulsed electric field treatment of microbial cells *J. Phys. D: Appl. Phys.* **39** 596
[41] Smith K C, Gowrishankar T R, Esser A T, Stewart D A and Weaver J C 2006 The spatially distributed dynamic transmembrane voltage of cells and organelles due to 10 ns pulses: meshed transport networks *IEEE Trans. Plasma Sci.* **34** 1394
[42] Puchar G, Kotnik T, Valic B and Miklavcic D 2006 Numerical determination of transmembrane voltage induced on irregularly shaped cells *Ann. Biomed. Eng.* **34** 642
[43] Joshi R P, Mishra A and Schoenbach K H 2008 Model assessment of cell membrane breakdown in clusters and tissues under high-intensity electric pulsing *IEEE Trans. Plasma Sci.* **36** 1680
[44] Babaeva Yu N, Bhoj A N and Kushner M J 2006 Streamer dynamics in gases containing dust particles *Plasma Source Sci. Technol.* **15** 591
[45] Hoath S B, Donnelly M M and Boissy R E 1990 Sensory transduction and the mammalian epidermis *Biosensors Bioelectron.* **5** 351
[46] Feldman Y, Ermolina I and Hayashi Y 2003 Time domain dielectric spectroscopy study of biological systems *IEEE Trans. Dielectr. Electr. Insul.* **10** 728
[47] Ermolina I, Polevaya Y, Feldman Y, Ginzburg B and Schlesinger M 2001 Study of normal and malignant white blood cells by time domain dielectric spectroscopy *IEEE Trans. Dielectr. Electr. Insul.* **8** 253
[48] Luque A and Ebert U 2008 Interacting streamers in air: the evolution of the space-charge layer in their heads *IEEE Trans. Plasma Sci.* **36** 914
[49] Xu X and Kushner M J 1999 The consequences of remnant surface charges on microdischarge spreading in dielectric barrier discharges *IEEE Trans. Plasma Sci.* **27** 108
[50] Xu X and Kushner M J 1998 Multiple microdischarge dynamics in dielectric barrier discharges *J. Appl. Phys.* **84** 4153
[51] Ayan H, Fridman G, Gutsol A F, Vasilets V N, Fridman A and Friedman G 2008 Nanosecond-pulsed uniform dielectric-barrier discharge *IEEE Trans. Plasma Sci.* **36** 504
[52] Ayan H, Staack D, Fridman G, Gutsol A, Mukhin Y, Starikovskii A, Fridman A and Friedman G 2009 Application of nanosecond-pulsed dielectric barrier discharge for biomedical treatment of topographically non-uniform surfaces *J. Phys. D: Appl. Phys.* **42** 125202